

Superconductivity in kagome metal YRu_3Si_2 with strong electron correlations

Chunsheng Gong, Shangjie Tian, Zhijun Tu, Qiangwei Yin, Yang Fu, Ruitao Luo, and Hechang Lei*
*Department of Physics and Beijing Key Laboratory of Opto-electronic Functional Materials & Micro-nano Devices,
Renmin University of China, Beijing 100872, China*

(Dated: September 24, 2021)

We report the detailed physical properties of YRu_3Si_2 with the Ru kagome lattice at normal and superconducting states. The results of resistivity and magnetization show that YRu_3Si_2 is a type-II bulk superconductor with $T_c \sim 3.0$ K. The specific heat measurement further suggests that this superconductivity could originate from the weak or moderate electron-phonon coupling. On the other hand, both large Kadawaki-Woods ratio and Wilson ratio indicate that there is a strong electron correlation effect in this system, which may have a connection with the featured flat band of kagome lattice.

I. INTRODUCTION

Due to the unique two-dimensional (2D) structure formed by corner-sharing triangles, the kagome lattice provides an exciting platform for studying magnetic frustration, electronic correlation and topological electronic state. Besides the long-sought spin liquid state in insulating magnetic kagome materials with strong geometrical frustration¹⁻⁴, the topological electronic structure in metallic kagome systems (kagome metals), such as Dirac point, flat band and von Hove point rooting in the special symmetry and arrangement of 2D kagome lattice, has also attracted much attention recently⁵⁻⁸. More importantly, the interplay between magnetism and band topology has resulted in the emergence of various exotic correlated topological phenomena and matters, such as giant anomalous Hall effect, massive Dirac fermions with large magnetic field tunability, magnetic Weyl semimetal state, and Chern gapped Dirac fermions with chiral edge state^{5,9-15}.

In contrast, the experimental studies on other electronic correlation effects intertwining with band topology in kagome metals are scarce due to the lack of material systems. The discovery of superconductivity and CDW state in AV_3Sb_5 ($A = \text{K}, \text{Rb}, \text{Cs}$) in very recent provide a novel platform to investigate such relationship¹⁶⁻¹⁹, which has been intensively studied in theory previously²⁰⁻²³. Moreover, the observed chiral charge order at high temperature and pair density wave state below superconducting transition temperature T_c further imply the intricate relationship between these correlated ordering states and non-trivial band topology^{24,25}.

In order to deepen the understanding of such correlated topological phenomena, it is necessary to explore other kagome metals harbouring superconductivity (kagome superconductors) But only a handful of kagome superconductors have been reported until now. One of examples is the Laves phase [cubic MgCu_2 (C15) type] superconductors with widely varying T_c ranging from 0.07 K to above 10 K²⁶⁻²⁸. However, since the strong interaction between kagome layer and other layers along the (111) direction of cubic Laves phase, the featured electronic

structure of 2D kagome lattice is strongly disturbed and the topological features of these materials become hard to discern. Another family of kagome superconductors is RTm_3B_2 ($R = \text{Y}, \text{La}, \text{Lu}, \text{Th}$ and $\text{Tm} = \text{Ru}, \text{Os}, \text{Rh}, \text{Ir}$) and RRu_3Si_2 with hexagonal layered CeCo_3B_2 structure in which transition metals form kagome layers²⁹. Among these materials, LaRu_3Si_2 with T_c as high as 7.8 K attracted lots of attention because it shows a typical band structure of kagome lattice and strong electron correlations which could be closely related to the kagome flat band³⁰⁻³⁴. When compared with LaRu_3Si_2 , except the structure and T_c value (~ 3 K - 3.5 K)^{30,35}, the physical properties of YRu_3Si_2 , especially superconducting properties, are still lacking. In this work, we carry out a detailed study on the physical properties of YRu_3Si_2 at normal and superconducting states. Experimental results indicate that YRu_3Si_2 is a weakly or moderately coupled BCS superconductor with strong electron correlations.

II. EXPERIMENTAL

YRu_3Si_2 polycrystal was synthesised using an arc-melting method. First, Y metal filing (99.9 %), Ru powder (99.9 %), and Si powder (99.9 %) with stoichiometric ratios were mixed, ground thoroughly and then pressed into a pellet using a hydraulic press in a glove box filled with argon atmosphere. In order to avoid the formation of YRu_2Si_2 , an amount of extra Ru was added, similar to the preparation of LaRu_3Si_2 ³². The pellet was arc-melted under argon atmosphere and remelted several times from both sides of the pellet to improve the homogeneity. Crystal structure and phase purity were examined by powder X-ray diffraction pattern (PXRD) with Cu K_α radiation ($\lambda = 0.15418$ nm) using a Bruker D8 X-ray diffractometer. The lattice parameters are extracted by fitting the PXRD pattern using the TOPAS4 software.³⁶ Electrical transport and specific heat measurements were performed in a Quantum Design PPMS-14T. Magnetization measurements were carried out in a Quantum Design MPMS3.

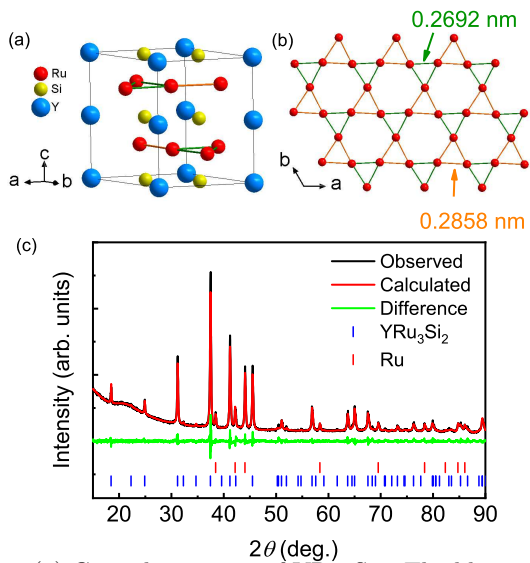


FIG. 1. (a) Crystal structure of YRu_3Si_2 . The blue, red and yellow balls represent Y, Ru and Si atoms, respectively. (b) Top view of the 2D distorted kagome lattice of Ru atoms. Two different bond distances are labelled with green and orange lines. (c) Powder XRD pattern and Rietveld refinement of YRu_3Si_2 polycrystal.

III. RESULTS AND DISCUSSION

Fig. 1(a) shows the crystal structure of YRu_3Si_2 , isostructural to LaRu_3Si_2 ³⁵. It is formed by stacking Y-Si and Ru layers alternately along the c axis. A key feature of this compound is the 2D distorted kagome layer formed by Ru atoms parallel to the ab plane. In this layer, there are two different Ru-Ru bond distances $d_{\text{Ru-Ru}}$ ($= 0.2692$ nm and 0.2858 nm). Meanwhile, the rotation of Ru triangles leads to the bond angle for collinear Ru atoms θ ($= 174.046^\circ$) deviating away from $\theta = 180^\circ$ in perfect kagome lattice (Fig. 1(b)). On the other hand, for Y-Si layer, the Y atoms form a triangle lattice when the Si atoms construct a honeycomb structure. Fig. 1(c) shows the PXRD pattern of YRu_3Si_2 and all peaks can be indexed well by the $P6_3/m$ space group (No. 176). The obtained lattice parameters by using Rietveld refinement are $a = 0.5542(1)$ nm and $c = 0.7150(7)$ nm, consistent with the reported values in literature³⁵. In addition to the diffraction peaks of YRu_3Si_2 , there are some extra peaks which originate from the excess of Ru in the raw material. A fitting result shows that the weight ratio of YRu_3Si_2 to Ru is about 84.1 : 15.9.

The temperature dependent magnetic susceptibility $4\pi\chi(T)$ with the zero field cooling (ZFC) and field cooling (FC) modes is shown in Fig. 2(a). A clear diamagnetic transition in $4\pi\chi(T)$ curve can be observed and confirms the occurrence of superconductivity in YRu_3Si_2 . The T_c determined from the ZFC $4\pi\chi(T)$ curve at $\mu_0 H = 1$ mT is about 2.98 K, close to the value reported previously³⁰. At $T = 1.8$ K, the estimated superconducting volume fraction is about 110 %, indicating a bulk superconduc-

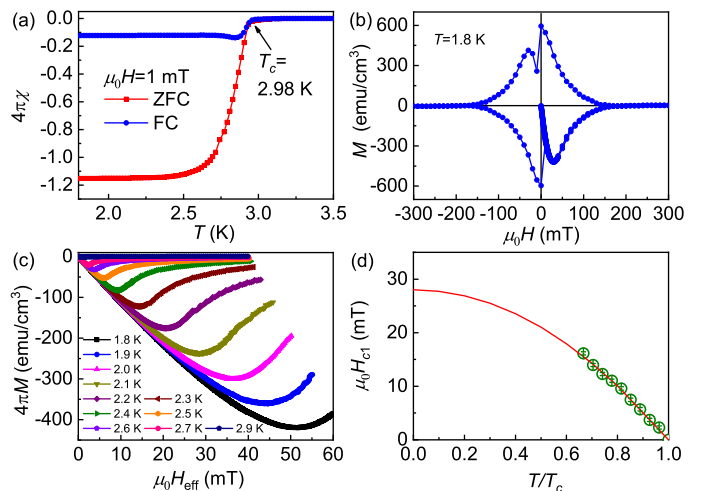


FIG. 2. (a) Temperature dependence of magnetic susceptibility $4\pi\chi(T)$ at 1 mT with ZFC and FC models. (b) Magnetization hysteresis loop for YRu_3Si_2 at 1.8 K. (c) Low-field dependence of magnetization $4\pi M(\mu_0 H)$ at various temperatures below T_c . (d) $\mu_0 H_{c1}$ as a function of T/T_c . The red line represents the fit using G-L equation.

tivity in YRu_3Si_2 . Compared with the ZFC $4\pi\chi(T)$ curve, a relatively weak diamagnetic signal of FC $4\pi\chi(T)$ curve due to flux pinning effect suggests that YRu_3Si_2 is a type-II superconductor. It is further confirmed by the magnetization hysteresis loop measured at 1.8 K (Fig. 2(b)). Moreover, the sudden jumps of $M(\mu_0 H)$ at low-field region can be ascribed to the entry of Meissner state. The initial magnetization as a function of magnetic field in the temperature range between 1.8 K and 2.9 K is shown in Fig. 2(c). All curves clearly fall on the same line and deviate from linearity at different temperatures. In order to estimate the lower critical field $\mu_0 H_{c1}$ correctly, the effective field $\mu_0 H_{\text{eff}}$ is calculated by using the formula $\mu_0 H_{\text{eff}} = \mu_0 H - N_d M$, where N_d is the demagnetization factor³⁷. Using the geometry size of rectangular sample, the calculated value of N_d is about 0.522³⁷. The $\mu_0 H_{c1}$ at each temperature is determined from the field where the $4\pi M(\mu_0 H)$ curve deviates from linearity ("Meissner line"). The obtained $\mu_0 H_{c1}$ as a function of reduced temperature T/T_c is shown in Fig. 2(d). The temperature dependence of $\mu_0 H_{c1}$ can be well fitted by the Ginzburg-Landau (G - L) equation $\mu_0 H_{c1}(T) = \mu_0 H_{c1}(0)[1 - (T/T_c)^2]$, where $\mu_0 H_{c1}(0)$ is the lower critical field at $T = 0$ K (red line). The fitted $\mu_0 H_{c1}(0)$ for YRu_3Si_2 is 28.0(3) mT.

Fig. 3(a) shows the temperature dependence of electrical resistivity $\rho(T)$ for YRu_3Si_2 polycrystal from 300 K to 2 K at zero field. The $\rho(T)$ decreases monotonically with decreasing temperature, indicating the metallic behavior of YRu_3Si_2 . The value of residual resistivity ratio (RRR) $\rho(300 \text{ K})/\rho(4 \text{ K})$ is about 8.6. Such relatively small value of RRR can be explained by the grain boundary effect in YRu_3Si_2 polycrystal. At high temperature the $\rho(T)$ curve exhibits a saturation tendency. This behavior could be described by the Ioffe-

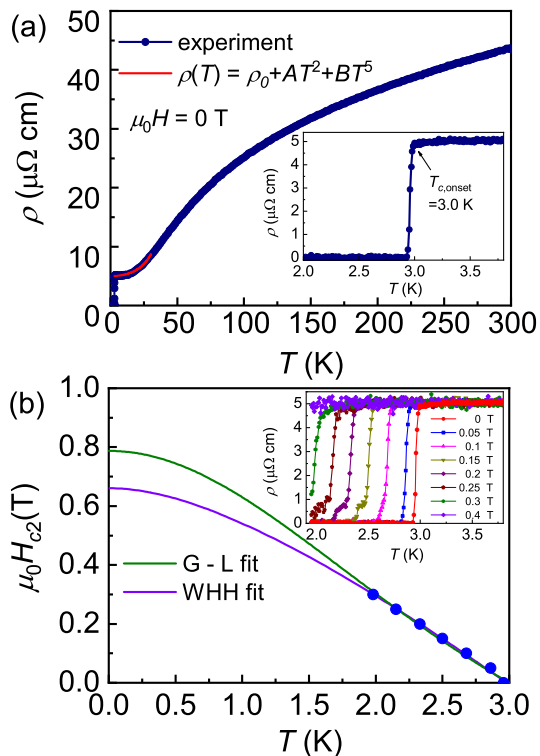


FIG. 3. (a) Temperature dependence of electrical resistivity $\rho(T)$ for YRu₃Si₂ polycrystal at zero field. The red solid line represents the fit using the formula $\rho(T) = \rho_0 + AT^2 + BT^5$. Inset: enlarged view of $\rho(T)$ curve near superconducting transition. (b) Temperature dependence of $\mu_0 H_{c2}(T)$. The green and purple lines represent the fits using the G - L and WHH formulas. Inset: $\rho(T)$ as a function of T at various magnetic fields.

Regel limit³⁸, e.g. the electron mean free path is close to the interatomic distance³⁹. At low temperature region ($T < 30$ K), the $\rho(T)$ curve can be well fitted using the formula $\rho(T) = \rho_0 + AT^2 + BT^5$, where ρ_0 is the residual resistivity, AT^2 and BT^5 term originates from the electron-electron and electron-phonon scattering, respectively (red line). The fit gives $\rho_0 = 4.99(5) \mu\Omega \text{ cm}$, $A = 2.38(7) \times 10^{-3} \mu\Omega \text{ cm K}^{-2}$ and $B = 5.9(4) \times 10^{-8} \mu\Omega \text{ cm K}^{-5}$. In addition, because the value of AT^2 is always larger than BT^5 at $T < 30$ K, the electron-electron scattering process dominates low-temperature resistivity. With lowering temperature further, a sharp superconducting transition can be observed at $T_{c,\text{onset}} = 3.0$ K with narrow transition width $\Delta T_c = 0.082$ K (inset of Fig. 3(a)). It is consistent with T_c obtained from the $4\pi\chi(T)$ curve. The small value of ΔT_c indicates the high quality of YRu₃Si₂ polycrystal.

In order to investigate the upper critical field $\mu_0 H_{c2}$ in YRu₃Si₂, the temperature dependence of $\rho(T)$ at various fields up to 0.4 T are measured (inset of Fig. 3(b)). The T_c shifts to lower temperature and the ΔT_c broadens slightly with increasing field. At $\mu_0 H = 0.4$ T, the superconducting transition can not be observed above 2 K. When defining the T_c as 50% drop from normal

state resistivity just above superconducting transition, the temperature dependence of $\mu_0 H_{c2}(T)$ for YRu₃Si₂ is plotted in Fig. 3(b). Using the G - L formula $\mu_0 H_{c2}(T) = \mu_0 H_{c2}(0)(T_{c,0}^2 - T^2)/(T_{c,0}^2 + T^2)$, where the $\mu_0 H_{c2}(0)$ is the zero-temperature upper critical field and $T_{c,0}$ is superconducting transition temperature at zero field. The fit (green line) gives $\mu_0 H_{c2}(0) = 0.78(2)$ T. On the other hand, when using the one-band Werthamer-Helfand-Hohenberg (WHH) formula (purple line)⁴⁰, the fitted $\mu_0 H_{c2}(0)$ is 0.655(2) T, close to the value obtained from the G-L formula. It is lower than that of LaRu₃Si₂ ($\mu_0 H_{c2}(0) \approx 4$ T)³². In addition, the $\mu_0 H_{c2}(0)$ is also much smaller than the Pauli paramagnetically limited field $\mu_0 H_{c2}^p (= 1.84 T_c = 5.52 \text{ T})$ ⁴¹, indicating that the orbital pairing-broken mechanism is dominant in YRu₃Si₂.

Using the fitted values of $\mu_0 H_{c1}(0) (= 28.0(3) \text{ mT})$ and $\mu_0 H_{c2}(0) (= 0.655(2) \text{ T})$, the zero-temperature superconducting characteristic parameters ξ_{GL} (coherence length) and λ_{GL} (penetration depth) can be estimated according to the following two equations $\xi_{\text{GL}} = (\frac{\phi_0}{2\pi\mu_0 H_{c2}(0)})^{\frac{1}{2}}$ and $\mu_0 H_{c1} = \frac{\phi_0}{4\pi\lambda_{\text{GL}}^2} \ln \frac{\lambda_{\text{GL}}}{\xi_{\text{GL}}}$, where ϕ_0 is the magnetic flux quantum ($h/2e = 2.07 \times 10^{-15} \text{ T m}^2$). The calculated value of ξ_{GL} and λ_{GL} is 22.43 (2) nm and 24.80(3) nm, respectively. Correspondingly, the derived GL parameter $\kappa_{\text{GL}} (= \lambda_{\text{GL}}/\xi_{\text{GL}})$ is 1.11(4), which is larger than $1/\sqrt{2}$. It confirms that YRu₃Si₂ is a type-II superconductor. The zero-temperature thermodynamic critical field $\mu_0 H_c(0)$ is obtained to be 0.42(9) T using the equation $\mu_0 H_c(0) = [\mu_0 H_{c1}(0)\mu_0 H_{c2}(0)/\ln \kappa_{\text{GL}}]^{1/2}$.

Fig. 4(a) shows the specific heat $C_p(T)$ of YRu₃Si₂ measured from 300 K to 2 K at zero field. At high temperature, consistent with the Dulong-Petit law, the $C_p(T)$ is close to the value of $3NR$ ($\sim 150 \text{ J mol}^{-1}\text{K}^{-1}$), where N ($= 6$) is the atomic numbers per formula and R ($= 8.314 \text{ J mol}^{-1}\text{K}^{-1}$) is the ideal gas constant, respectively. At low temperature, a specific heat jump can be observed clearly due to the superconducting transition. It also confirms the bulk nature of superconductivity in YRu₃Si₂ (Fig. 4(b)). With increasing field, this jump shifts to lower temperature accompanying with the decrease of height. On the other hand, at $\mu_0 H = 0.5$ T where the superconducting transition is suppressed below 2 K, the relationship of C_p/T and T^2 can not be described by a linear behavior (inset of Fig. 4(c)) and this suggests that there may be an anomalous contribution of high-frequency phonons³². Thus, the low-temperature $C_p(T)$ at $\mu_0 H = 0.5$ T is fitted using the formula $C_p = \gamma T + \beta T^3 + \eta T^5$, where the first item is the specific heat of electrons at normal state with the Sommerfeld coefficient γ , and the last two items represent the lattice specific heat when considering the contribution of high-frequency phonons⁴². The fit gives $\gamma = 27.5(8) \text{ mJ mol}^{-1}\text{K}^{-2}$, $\beta = 0.12(2) \text{ mJ mol}^{-1}\text{K}^{-4}$ and $\eta = 0.00141(7) \text{ mJ mol}^{-1}\text{K}^{-6}$. By using the formula $\Theta_D = (12\pi^4 NR/5\beta)^{1/3}$, the calculated Debye temperature Θ_D is 460(26) K. It is larger than the value in LaRu₃Si₂ ($\Theta_D = 412$ K) derived using the same method³², possibly due to the smaller atomic mass of Y than La.

TABLE I. Physical parameters of YRu₃Si₂.

Parameter	Units	Value
T_c	K	3.0
RRR	-	8.6
ρ_0	$\mu\Omega$ cm	4.99(5)
A	$\mu\Omega$ cm K ⁻²	$2.38(7)\times 10^{-3}$
B	$\mu\Omega$ cm K ⁻⁵	$5.9(4)\times 10^{-8}$
$\mu_0 H_{c1}(0)$	mT	28.0(3)
$\mu_0 H_{c2}(0)$	T	0.655(2)
$\mu_0 H_c(0)$	T	0.42(9)
ξ_{GL}	nm	22.43(2)
λ_{GL}	nm	24.80(3)
κ_{GL}	-	1.11(4)
γ	mJ mol ⁻¹ K ⁻²	27.5(8)
β	mJ mol ⁻¹ K ⁻⁴	0.12(2)
η	mJ mol ⁻¹ K ⁻⁶	0.00141(7)
$\Delta C_{ele}/\gamma T_c$	-	1.21(4)
Θ_D	K	460(26)
λ_{e-ph}	-	0.50(2)
$\chi(0)$	emu mol ⁻¹ Oe ⁻¹	$5.56(2)\times 10^{-4}$
T_E	K	640(10)
C	emu K mol ⁻¹ Oe ⁻¹	0.01393(7)
T_0	K	1.38(2)
A/γ^2	$\mu\Omega$ cm mol ² K ² J ⁻²	3.15(2)
R_w	-	1.49(4)

The specific heat of electrons C_{ele} can be obtained by subtracting the phonon contribution from the total specific heat (Fig. 4(d)). According to the method of equal-entropy construction (blue solid lines), the thermodynamic T_c is determined to be 2.84 K, consistent with the values obtained from the $\rho(T)$ and $\chi(T)$ curves. The specific heat jump $\Delta C_{ele}/\gamma T_c$ at T_c is 1.21(4) which is smaller than the value of weak-coupling limit 1.43. It implies that YRu₃Si₂ might be a weak- or moderate-coupling superconductor. It has to be noted that the existence of Ru impurity could also contribute to the reduced specific heat jump. Using the obtained Θ_D and T_c , the electron-phonon coupling constant λ_{e-ph} can be calculated according to the McMillan equation⁴³,

$$\lambda_{e-ph} = \frac{1.04 + \mu^* \ln\left(\frac{\Theta_D}{1.45T_c}\right)}{(1 - 0.62\mu^*) \ln\left(\frac{\Theta_D}{1.45T_c}\right) - 1.04} \quad (1)$$

where μ^* is the Coulomb pseudopotential parameter. Taken $\mu^* = 0.13$ as for many intermetallic superconductors, the calculated value of λ_{e-ph} is 0.50(2), further confirming that YRu₃Si₂ is a weak- or moderate-coupling superconductor. All of physical parameters of YRu₃Si₂ are listed in Table I.

5

In order to get more information about electron correlation effect in YRu₃Si₂, temperature dependence of $\chi(T)$

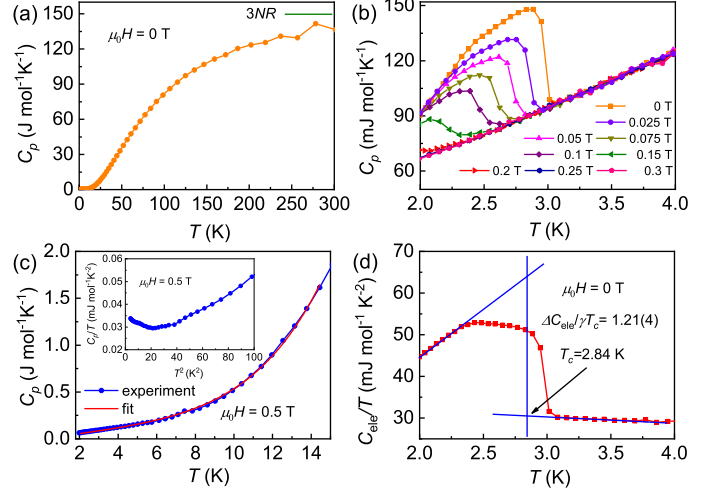


FIG. 4. (a) Temperature dependence of zero-field $C_p(T)$ from 300 K to 2 K. (b) C_p vs T at various magnetic fields. (c) Temperature dependence of $C_p(T)$ at $\mu_0 H = 0.5$ T. The red solid line represents the fit using the formula $C_p = \gamma T + \beta T^3 + \eta T^5$. Inset: C_p/T vs T^2 at $\mu_0 H = 0.5$ T. (d) C_{ele}/T as a function of T at zero field.

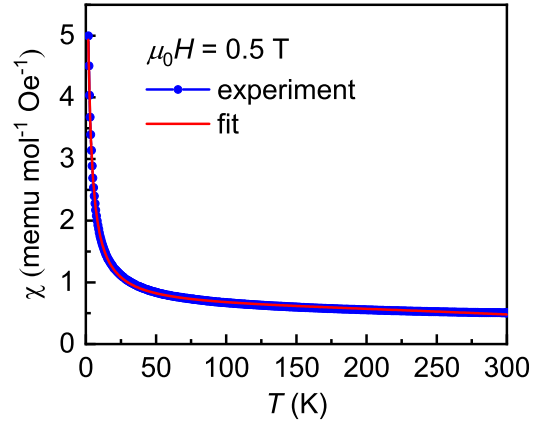


FIG. 5. Temperature dependence of $\chi(T)$ measured at $\mu_0 H = 0.5$ T with ZFC mode. The red solid line presents the fit using the formula $\chi(T) = \chi(0)[1 - (T/T_E)^2] + C/(T + T_0)$.

at $\mu_0 H = 0.5$ T with ZFC mode is measured (Fig. 5). YRu₃Si₂ shows a paramagnetic behavior from 300 K to 2 K and no long-range magnetic translation is observed. In addition, it is found that the $\chi(T)$ curve can be well fitted using the following expression as in LaRu₃Si₂³²,

$$\chi(T) = \chi(0)\left[1 - \left(\frac{T}{T_E}\right)^2\right] + \frac{C}{T + T_0} \quad (2)$$

Here, the first term represents the Pauli susceptibility related to the density of state at the Fermi energy level E_F . The T_E represents a parameter proportional to the E_F . The second term refers to the weak magnetic contribution that may be caused by the local moment. The

fit gives $\chi(0) = 5.56(2) \times 10^{-4}$ emu mol⁻¹ Oe⁻¹, $T_E = 640(10)$ K, $C = 0.01393(7)$ emu K mol⁻¹ Oe⁻¹ and $T_0 = 1.38(2)$ K. On the other hand, the Kadawaki-Woods ratio A/γ^2 and the Wilson ratio $R_W = 4\pi^2 k_B^2 \chi(0)/3(g\mu_B)^2 \gamma$ are often used to characterize the strength of electron correlations, where g is Lande factor which takes about 2 for an electron and μ_B is the Bohr magneton^{44,45}. Using above values of $A = 2.38(7) \times 10^{-3}$ $\mu\Omega$ cm, $\gamma = 27.5(8)$ mJ mol⁻¹ K⁻² and $\chi(0) = 5.56(2) \times 10^{-4}$ emu mol⁻¹ Oe⁻¹, the calculated A/γ^2 and the R_W is $3.15(2)$ $\mu\Omega$ cm mol² K² J⁻² and $1.49(4)$, respectively (summarized in Table I). The value of A/γ^2 is much larger than those in transition metals (0.4 $\mu\Omega$ cm mol² K² J⁻²) and relatively smaller than the universal value 10 $\mu\Omega$ cm mol² K² J⁻² in heavy-fermion systems^{44,46}. The value of R_W is larger than 1 that is expected in noninteracting free electron gas. Both large A/γ^2 and R_W suggest strong electron correlations in YRu₃Si₂.

IV. CONCLUSION

In summary, kagome metal YRu₃Si₂ shows a superconducting transition at $T_c \sim 3.0$ K. The zero-temperature

$\mu_0 H_{c1}(0)$ and $\mu_0 H_{c2}(0)$ is $28.0(3)$ mT and $0.655(2)$ T, respectively. The derived κ_{GL} is $1.11(4)$, confirming that YRu₃Si₂ is a type-II superconductor. Moreover, the relatively small $\Delta C_{ele}/\gamma T_c$ and λ_{e-ph} indicates that YRu₃Si₂ has a weakly or moderately coupled BCS bulk superconductivity. On the other hand, rather strong electron correlation effect is identified by the large values of A/γ^2 and R_W . This could be related to the existence of kagome flat band in YRu₃Si₂, which can result in high density of states near the E_F .

V. ACKNOWLEDGEMENTS

This work was supported by National Key R&D Program of China (Grant No. 2018YFE0202600), Beijing Natural Science Foundation (Grant No. Z200005), National Natural Science Foundation of China (Grant No. 11822412 and 11774423), the Fundamental Research Funds for the Central Universities and Research Funds of Renmin University of China (RUC) (Grant No. 18XNLG14, 19XNLG13, 19XNLG17 and 20XNH062), Outstanding Innovative Talents Cultivation Funded Programs 2020 of Renmin University of China, and Beijing National Laboratory for Condensed Matter Physics.

-
- * hlei@ruc.edu.cn
- ¹ L. Balents, *Nature* **464**, 199 (2010).
 - ² C. Broholm, R. J. Cava, S. A. Kivelson, D. G. Nocera, M. R. Norman, and T. Senthil, *Science* **367**, 6475 (2020).
 - ³ M. P. Shores, E. A. Nytko, B. M. Bartlett, and D. G. Nocera, *J. Am. Chem. Soc.* **127**, 13462 (2005).
 - ⁴ T. H. Han, J. S. Helton, S. Chu, D. G. Nocera, J. A. Rodriguez-Rivera, C. Broholm, and Y. S. Lee, *Nature* **492**, 406 (2012).
 - ⁵ L. Ye, M. Kang, J. Liu, F. von Cube, C. R. Wicker, T. Suzuki, C. Jozwiak, A. Bostwick, E. Rotenberg, D. C. Bell, L. Fu, R. Comin, and J. G. Checkelsky, *Nature* **555**, 638 (2018).
 - ⁶ M. Kang, L. Ye, S. Fang, J.-S. You, A. Levitan, M. Han, J. I. Facio, C. Jozwiak, A. Bostwick, E. Rotenberg, M. K. Chan, R. D. McDonald, D. Graf, K. Kaznatcheev, E. Vescovo, D. C. Bell, E. Kaxiras, J. van den Brink, M. Richter, M. P. Ghimire, J. G. Checkelsky, and R. Comin, *Nat. Mater.* **19**, 163 (2020).
 - ⁷ Z. H. Liu, M. Li, Q. Wang, G. W. Wang, C. H. P. Wen, K. Jiang, X. L. Lu, S. C. Yan, Y. B. Huang, D. W. Shen, J.-X. Yin, Z. Q. Wang, Z. P. Yin, H. C. Lei, and S. C. Wang, *Nat. Commun.* **11**, 4002 (2020).
 - ⁸ M. Kang, S. Fang, L. Ye, H. C. Po, J. Denlinger, C. Jozwiak, A. Bostwick, E. Rotenberg, E. Kaxiras, J. G. Checkelsky, and R. Comin, *Nat. Commun.* **11**, 4004 (2020).
 - ⁹ S. Nakatsuji, N. Kiyohara, and T. Higo, *Nature* **527**, 212 (2015).
 - ¹⁰ A. K. Nayak, J. E. Fischer, Y. Sun, B. Yan, J. Karel, A. C. Komarek, C. Shekhar, N. Kumar, W. Schnelle, J. Kübler, C. Felser, and S. S. P. Parkin, *Sci. Adv.* **2**, e1501870 (2016).
 - ¹¹ Q. Wang, S. S. Sun, X. Zhang, F. Pang, and H. C. Lei, *Phys. Rev. B* **94**, 075135 (2016).
 - ¹² E. Liu, Y. Sun, N. Kumar, L. Muechler, A. Sun, L. Jiao, S. Y. Yang, D. Liu, A. Liang, Q. Xu, J. Kroder, V. Süß, H. Borrmann, C. Shekhar, Z. Wang, C. Xi, W. Wang, W. Schnelle, S. Wirth, Y. Chen, S. T. B. Goennenwein, and C. Felser, *Nat. Phys.* **14**, 1125 (2018).
 - ¹³ Q. Wang, Y. F. Xu, R. Lou, Z. H. Liu, M. Li, Y. B. Huang, D. W. Shen, H. M. Weng, S. C. Wang, and H. C. Lei, *Nat. Commun.* **9**, 3681 (2018).
 - ¹⁴ J. X. Yin, S. S. Zhang, H. Li, K. Jiang, G. Chang, B. Zhang, B. Lian, C. Xiang, I. Belopolski, H. Zheng, T. A. Cochran, S. Y. Xu, G. Bian, K. Liu, T. R. Chang, H. Lin, Z. Y. Lu, Z. Wang, S. Jia, W. Wang, and M. Z. Hasan, *Nature* **562**, 91 (2018).
 - ¹⁵ J. X. Yin, W. Ma, T. A. Cochran, X. Xu, S. S. Zhang, H. J. Tien, N. Shumiya, G. Cheng, K. Jiang, B. Lian, Z. Song, G. Chang, I. Belopolski, D. Multer, M. Litskevich, Z. J. Cheng, X. P. Yang, B. Swidler, H. Zhou, H. Lin, T. Neupert, Z. Wang, N. Yao, T. R. Chang, S. Jia, and M. Z. Hasan, *Nature* **583**, 533 (2020).
 - ¹⁶ B. R. Ortiz, L. C. Gomes, J. R. Morey, M. Winiarski, M. Bordelon, J. S. Mangum, I. W. H. Oswald, J. A. Rodriguez-Rivera, J. R. Neilson, S. D. Wilson, E. Ertekin, T. M. McQueen, and E. S. Toberer, *Phys. Rev. Mater.* **3**, 094407 (2019).
 - ¹⁷ B. R. Ortiz, S. M. L. Teicher, Y. Hu, J. L. Zuo, P. M. Sarte, E. C. Schueller, A. M. M. Abeykoon, M. J. Krogstad, S. Rosenkranz, R. Osborn, R. Seshadri, L. Balents, J. F. He, and S. D. Wilson, *Phys. Rev. Lett.* **125**, 247002 (2020).
 - ¹⁸ B. R. Ortiz, P. M. Sarte, E. M. Kenney, M. J. Graf, S. M. L. Teicher, R. Seshadri, and S. D. Wilson, *Phys. Rev.*

- Mater. **5**, 034801 (2021).
- ¹⁹ Q. W. Yin, Z. J. Tu, C. S. Gong, Y. Fu, S. H. Yan, and H. C. Lei, *Chin. Phys. Lett.* **38**, 037403 (2021).
- ²⁰ W.-H. Ko, P. A. Lee, and X.-G. Wen, *Phys. Rev. B* **79**, 214502 (2009).
- ²¹ W.-S. Wang, Z.-Z. Li, Y.-Y. Xiang, and Q.-H. Wang, *Phys. Rev. B* **87**, 115135 (2013).
- ²² M. L. Kiesel, C. Platt, and R. Thomale, *Phys. Rev. Lett.* **110**, 126405 (2013).
- ²³ I. I. Mazin, H. O. Jeschke, F. Lechermann, H. Lee, M. Fink, R. Thomale, and R. Valentí, *Nat. Commun.* **5**, 4261 (2014).
- ²⁴ Y.-X. Jiang, J.-X. Yin, M. M. Denner, N. Shumiya, B. R. Ortiz, J. He, X. Liu, S. S. Zhang, G. Chang, I. Belopolski, Q. Zhang, M. S. Hossain, T. A. Cochran, D. Multer, M. Litskevich, Z.-J. Cheng, X. P. Yang, Z. Guguchia, G. Xu, Z. Wang, T. Neupert, S. D. Wilson, and M. Z. Hasan, *arXiv: 2012.15709* (2020).
- ²⁵ H. Chen, H. Yang, B. Hu, Z. Zhao, J. Yuan, Y. Xing, G. Qian, Z. Huang, G. Li, Y. Ye, Q. Yin, C. Gong, Z. Tu, H. Lei, S. Ma, H. Zhang, S. Ni, H. Tan, C. Shen, X. Dong, B. Yan, Z. Wang, and H.-J. Gao, *arXiv: 2103.09188* (2021).
- ²⁶ Ö. Rapp, J. Invarsson, and T. Claesson, *Phys. Lett. A* **50**, 159 (1974).
- ²⁷ S. S. Sun, K. Liu, and H. C. Lei, *J. Phys.: Condens. Matter* **28**, 085701 (2016).
- ²⁸ C. S. Gong, Q. Wang, S. H. Wang, and H. C. Lei, *J. Phys.: Condens. Matter* **32**, 295601 (2020).
- ²⁹ H. C. Ku, G. P. Meisner, F. Acker, and D. C. Johnston, *Solid State Commun.* **35**, 91 (1980).
- ³⁰ H. Barz, *Mater. Res. Bull.* **15**, 1489 (1980).
- ³¹ M. Escorne, A. Mauger, L. C. Gupta, and C. Godart, *Phys. Rev. B* **49**, 12051 (1994).
- ³² S. Li, B. Zeng, X. G. Wan, J. Tao, F. Han, H. Yang, Z. H. Wang, and H. H. Wen, *Phys. Rev. B* **84**, 214527 (2011).
- ³³ B. X. Li, S. Li, and H. H. Wen, *Phys. Rev. B* **94**, 094523 (2016).
- ³⁴ C. Mielke, III, Y. Qin, J. X. Yin, H. Nakamura, D. Das, K. Guo, R. Khasanov, J. Chang, Z. Q. Wang, S. Jia, S. Nakatsuji, A. Amato, H. Luetkens, G. Xu, M. Z. Hasan, and Z. Guguchia, *Phys. Rev. Mater.* **5**, 034803 (2021).
- ³⁵ J. M. Vandenberg and H. Barz, *Mater. Res. Bull.* **15**, 1493 (1980).
- ³⁶ TOPAS Version 4; Bruker AXS, Karlsruhe, Germany (2007).
- ³⁷ A. Aharoni, *J. Appl. Phys.* **83**, 3432 (1998).
- ³⁸ A. F. Ioffe and A. R. Regel, *Prog. Semicond.* **4**, 237 (1961).
- ³⁹ V. N. Zverev, A. V. Korobenko, G. L. Sun, D. L. Sun, C. T. Lin, and A. V. Boris, *JETP Lett.* **90**, 130 (2009).
- ⁴⁰ N. R. Werthamer, E. Helfand, and P. C. Hohenberg, *Phys. Rev.* **147**, 295 (1966).
- ⁴¹ K. Maki, *Phys. Rev.* **148**, 362 (1966).
- ⁴² H. D. Yang and J. Y. Lin, *J. Phys. Chem. Solids* **62**, 1861 (2001).
- ⁴³ W. L. McMillan, *Phys. Rev.* **167**, 331 (1968).
- ⁴⁴ K. Kadowaki and S. B. Woods, *Solid State Commun.* **58**, 507 (1986).
- ⁴⁵ K. G. Wilson, *Rev. Mod. Phys.* **47**, 773 (1975).
- ⁴⁶ A. C. Jacko, J. O. Fjærestad, and B. J. Powell, *Nat. Phys.* **5**, 422 (2009).